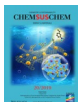# Hydrogenation of Functionalized Nitroarenes Catalyzed by Single-Phase Pyrite FeS$_2$ Nanoparticles on N,S-Codoped Porous Carbon

Yanan Duan,[a] Xiaosu Dong,[a] Tao Song,[a] Zhaozhan Wang,[a] Jianliang Xiao,[b] Youzhu Yuan,[c] and Yong Yang*[a]

Catalytic hydrogenation of nitroarenes is an industrially very important and environmentally friendly process for the production of anilines; however, highly chemoselective reduction of nitroarenes decorated with one or more reducible groups in a nitroarene molecule remains a challenge. Herein, a novel hybrid non-noble iron-based nanocatalyst (named as FeS$_2$/NSC) was developed, which was prepared from biomass as C and N source together with inexpensive Fe(NO$_3$)$_3$ as Fe source through high-temperature pyrolysis in a straightforward and cost-effective procedure. Comprehensive characterization revealed that single-phase pyrite FeS$_2$ nanoparticles with precisely defined composition and uniform size were homogeneously dispersed on N,S-codoped porous carbon with large specific surface area, hierarchical porous channels, and high pore volume. The resultant catalyst FeS$_2$/NSC demonstrated good catalytic activity for hydrogenation of functionalized nitroarenes with good tolerance of various functional groups in water as a sustainable and green solvent. Compared with bulk pyrite FeS$_2$ and other non-noble metal-based heterogeneous catalysts reported in the literature, a remarkably enhanced activity was observed under mild reaction conditions. More importantly, FeS$_2$/NSC displayed exclusive chemoselectivity for the reduction of nitro groups for nitroarenes bearing varying readily reducible groups.

Introduction

Functionalized anilines are industrially important intermediates for a variety of specialty and fine chemicals as well as key building blocks for high-performance rubbers and polymers.[1] In particular, structurally complex anilines decorated with diverse functional groups have widespread applications in life science. To date, more than 4 000 000 tons of aniline and its derivatives have been produced per year over the worldwide markets.[2] However, chemoselective hydrogenation of the nitro group still remains a great challenge if the nitroarene molecule bears readily reducible functional groups, such as C=C, C≡C, C=O, and C≡N. Specifically, precious-metal-based catalysts generally give high activity but only low selectivity to the desired amines. Since the breakthrough of gold-based catalysts for se-

lective hydrogenation of 3-nitrostyrene was reported by Corma and Serna in 2006,[3] significant progress toward improved selectivity has been achieved. Various metal-based catalysts (e.g., platinum,[4] silver,[5] palladium,[6] rhodium,[7] and gold[8]) have been developed through different preparation strategies, such as adding surface modifiers, tailoring the metal-particle sizes, alloying with second-component metals, controlling metal–support interaction, or fabricating unique core–shell or well-confined nanostructured catalysts. Nevertheless, the high cost and scarcity of these precious metals accompanied with complicated and tedious preparation procedures significantly hamper their practical potential, especially for large-scale industrial applications. Therefore, the development of more earth-abundant alternatives with high catalytic efficiency and excellent chemoselectivity is highly desirable. Besides, a facile and environmentally friendly process to prepare such non-noble metal-based catalyst with high stability is also of great importance from both economic and sustainable viewpoints.

The sustainable, copious supply of non-noble metal salts, especially iron, coupled with their environmentally benign nature and low toxicity, makes them appealing catalysts. In this context, Beller and co-workers have made significant achievements and developed nanosized iron- or cobalt-based metal/metal oxide catalysts for highly selective hydrogenation of functionalized nitroarenes.[9] However, in their cases, relatively demanding reaction conditions such as long reaction time (> 12 h), high temperature (> 120 °C), high H$_2$ pressure (50 bar), and toxic and flammable organic solvents are usually required to obtain satisfactory reaction efficiency, although the catalysts

[a] Y. Duan, Dr. X. Dong, Dr. T. Song, Z. Wang, Prof. Y. Yang
Qingdao Institute of Bioenergy and Bioprocess Technology,
Chinese Academy of Sciences
Qingdao 266101 (P.R. China)
E-mail: yangyong@qibebt.ac.cn

[b] Prof. J. Xiao
Department of Chemistry
Liverpool University
Liverpool L69 7ZD (UK)

[c] Prof. Y. Yuan
State Key Laboratory of Physical Chemistry of Solid Surfaces, National Engineering Laboratory for Green Chemical Production of Alcohols-Ethers-Ethers, College of Chemistry and Chemical Engineering
Xiamen University
Xiamen 361005 (P.R. China)

Supporting Information and the ORCID identification number(s) for the author(s) of this article can be found under:
https://doi.org/10.1002/cssc.201901867.

feature good tolerance of functional groups with excellent selectivity. In addition to the relatively harsh reaction conditions, structurally sophisticated and expensive organic ligands are a prerequisite for fabricating those well-defined iron- or cobalt-based catalysts with strong ligand-dependent catalytic performance. Such limitations spurred us to develop a novel inexpensive non-noble metal catalyst with facile preparation procedure that can allow for a general reduction of all kinds of nitroarenes with superior catalytic efficiency and outstanding selectivity and with water as a green, non-toxic, and non-flammable solvent under mild reaction conditions.

Recently, cubic pyrite-type transition-metal disulfides (MS_2, M = Fe, Co, Ni) with very diverse and intriguing properties have attracted considerable attention. Amongst the family of transition-metal pyrites, iron disulfide (FeS_2), an inexpensive and earth-abundant mineral commonly known as fool's gold has demonstrated exceptionally high promise in numerous cutting-edge energy technologies, such as solar cells, lithium/sodium-ion batteries, electrocatalytic hydrogen and oxygen evolution, and oxygen reduction.[10] However, to date, the investigation of FeS_2 or other pyrites as catalyst for organic transformations is still limited, and only sporadic studies are available.[11, 12] For instance, Schaak and co-workers and Keil and co-workers independently investigated bulk FeS_2 or FeS_2 nanoparticles as catalyst for the selective hydrogenation of nitroarenes.[11] In both cases, nitroarenes bearing C=C and other functional groups could be converted to the corresponding amines with full selectivity at complete conversion; however, complete selectivity for 4-iodonitrobenzene, one of the most demanding substrates, was obtained only at ≤75% conversion, indicating the possibility of dehalogenation at higher conversion. Nonetheless, despite the easy availability, good biocompatibility, and low price of pyrite FeS_2 as well as the generally good selectivity for hydrogenation of nitroarenes, the overall activities achieved so far are very poor and need to be further improved. Furthermore, the presence of iron oxides on the surface of the as-prepared bulk FeS_2 also raises the question of which phase actually is the active catalyst, which needs to be elucidated by formation of a single-phase pyrite FeS_2 in the catalyst. However, the synthesis of single-phase pyrite FeS_2 with precisely defined composition remains challenging. Specifically, demanding preparation conditions are necessary owing to unavoidable segregation of Fe and S species, which generally causes changes of the variation of the stoichiometry, crystalline structure, and material phase, thereby substantially influencing its photovoltaic efficiency and catalytic performance.[13]

Our recent studies and other previous reports have demonstrated that the hybridization of the non-noble metal catalysts, such as cobalt, nickel, and iron, with heteroatom-doped porous carbon can lead to improved catalytic activity and selectivity as well as stability in catalysis.[14] The enhancement of catalytic performance was attributed to the synergistic effect of chemical compositions (appropriate N-, P-, or S-doping) and unique porous structures (large specific surface area, high pore volume, hierarchical porous channels). We envisioned that a boosted reaction efficiency could be expected if a nanosized

hybrid pyrite catalyst, composed of FeS_2 nanoparticles and heteroatom-doped porous carbon materials, was fabricated; however, such an investigation has not been explored before.

Herein we report, for the first time, the fabrication of novel single-phase pyrite FeS_2 nanoparticles (NPs) supported on N,S-codoped hierarchical porous carbon (FeS_2/NSC) as highly active and stable catalyst for chemoselective hydrogenation of functionalized nitroarenes. FeS_2/NSC was prepared through a facile three-step (hydro-)thermal process, employing naturally renewable and easily available biomass as N and C sources together with earth-abundant and low-cost iron salt as starting materials, in an operationally simple, environmentally benign, and cost-effective manner. FeS_2/NSC can selectively hydrogenate a broad spectrum of functionalized nitroarenes into more versatile and valuable anilines with water as the solvent under mild conditions (2.0 MPa H_2, 120 °C). Compared with unsupported bulk FeS_2, FeO_x, and even other non-noble metal-based heterogeneous catalysts reported in the literature[9], a remarkably enhanced catalytic activity with exclusive selectivity was achieved. Characterization studies revealed that single-phase FeS_2 NPs with uniform size and precisely defined composition were homogeneously dispersed on N,S-codoped porous carbon, and FeS_2/NSC possesses a large specific surface area, hierarchical porous channels, and a high pore volume with strong interaction between FeS_2 NPs and support. DFT calculations disclosed that FeS_2/NSC has a preferential adsorption capacity for the nitro group, which accounts for the enhanced catalytic activity and exclusive chemoselectivity. Furthermore, FeS_2/NSC could be readily recovered for several reuses without an appreciable loss in catalytic performance, highlighting its practical potential.

Results and Discussion

Preparation and characterization of FeS_2/NSC

FeS_2/NSC was synthesized in a sequential hydrothermal, pyrolysis, and sulfurization procedure as shown in Scheme 1 (see details in the Supporting Information). First, fresh bamboo shoots were cut into slices, dried, and ground into powder, followed by the hydrothermal process to get a brown hydrochar solid. Second, the resultant solid was homogeneously mixed with $Fe(NO_3)_3$, followed by pyrolysis under N_2 atmosphere at 800 °C for 2 h to get black powder, labeled as FeO_x/NC. Subsequently, FeS_2/NSC was obtained by annealing FeO_x/NC with sublimed sulfur at 500 °C with a heating rate of 5 °C min^{-1} for 2 h in an N_2 atmosphere. The iron content in FeS_2/NSC was determined to be 6.8 wt% by inductively coupled plasma optical emission spectrometry (ICP-OES), and N and S contents were estimated to be 3.07 and 26.75 wt%, respectively, by elemental analysis.

The powder XRD pattern of FeS_2/NSC (Figure 1A) shows that all diffraction peaks, exclusively indexed to the (1 1 1), (2 0 0), (2 1 0), (2 1 1), (2 2 0), (3 1 1), (2 2 2), (0 2 3), and (3 2 1) facets, respectively, were clearly observed, in good line with a cubic FeS_2 (JCPDS No. 42-1340; space group $Pa\bar{3}$, $a = b = c = 5.4179$ Å). No other peaks from impurities such as marcasite FeS_2 or hexagonal troilite FeS could be detected. The average
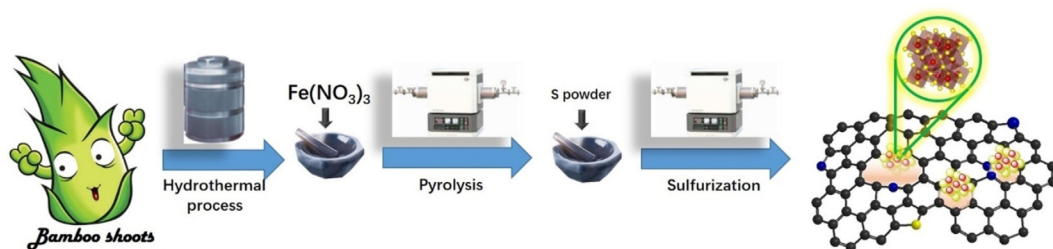
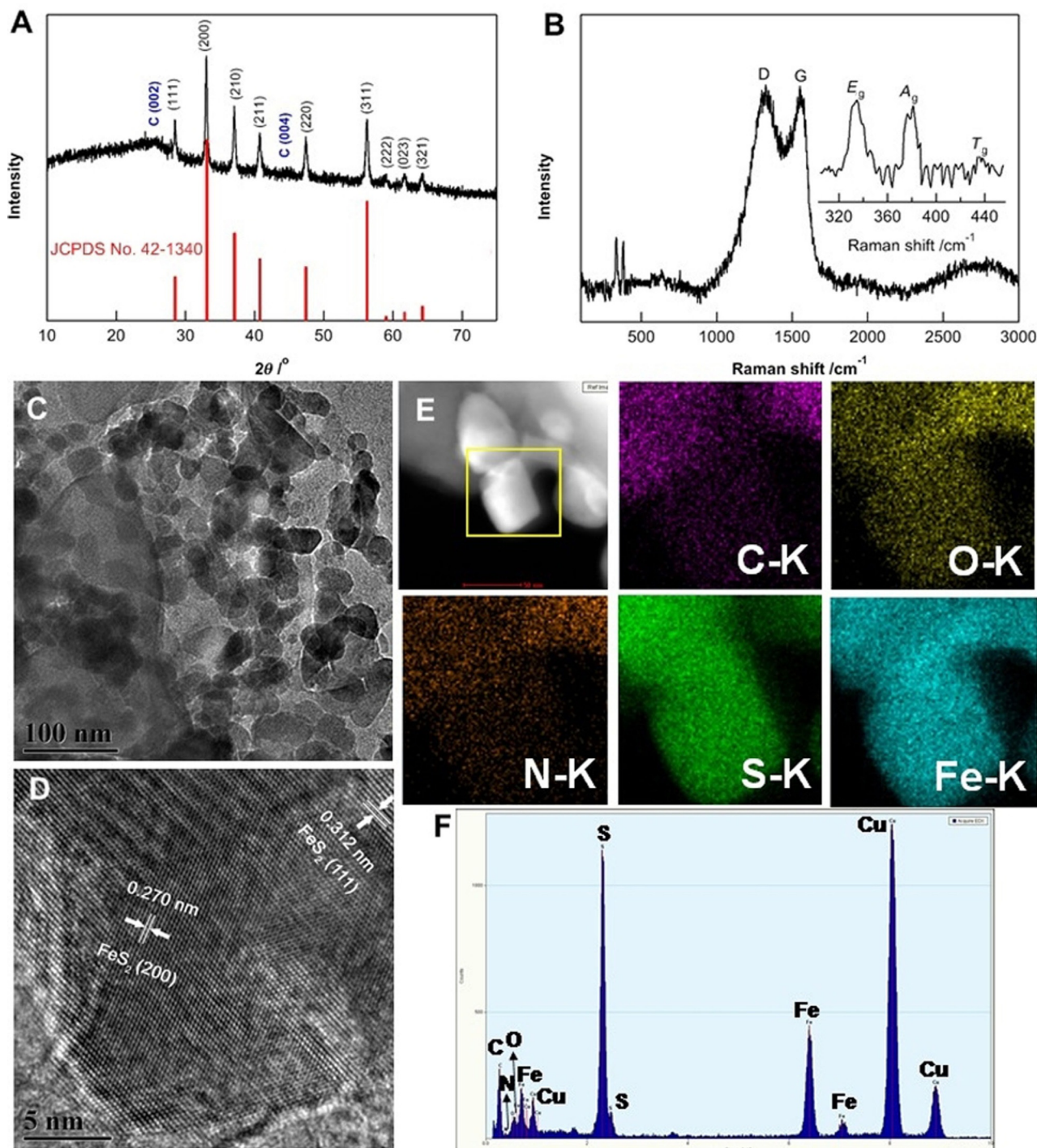**Scheme 1.** Illustration of the preparation of FeS₂/NSC.

Figure 1. (A) XRD pattern and (B) Raman spectrum of FeS₂/NSC. (C, D) HR-TEM and (E) HAADF-STEM images and EDX mappings of C, O, N, S, and Fe for FeS₂/NSC. (F) EDX analysis result for FeS₂/NSC.

lattice constant of the pyrite FeS_2 NPs was found to be 5.424 Å, in agreement with stoichiometric pyrite. Besides, two characteristic diffraction peaks with less intensity at 26.2 and 44.0° corresponding to the (002) and (004) facets of graphitic carbon were also observed, indicating the formation of graphitic carbon in the sample. The Raman spectrum verified the formation of graphitic carbon in the catalyst FeS_2/NSC through the appearance of two clear peaks at 1590 and 1350 cm^{-1} (Figure 1B). The peak at 1350 cm^{-1} is attributable to the D band for the disordered carbon, edge defects, and other defects, whereas the peak at 1590 cm^{-1} corresponds to the G band for the vibrational mode in the sp^2-bonded graphitic carbon.[15] Moreover, three peaks located at 332, 377, and 430 cm^{-1} were also detected, which are the characteristic active modes for bulk pyrite FeS_2 corresponding to the S_2 vibration (E_g), S—S in-phase stretch (A_g), and stretch (T_g) modes,[16] respectively. This observation further confirms the formation of single-phase pyrite in the sample.

TEM imaging disclosed that FeS_2 NPs with rather uniform sizes of (30 ± 10) nm were evenly distributed on the surface of carbon support (Figure 1C). The high-resolution (HR-)TEM image presents lattice fringes with interplanar spacings of 0.270 and 0.312 nm, corresponding to the (200) and (111) crystal planes of pyrite FeS_2 (Figure 1D). The homogeneous distribution of FeS_2 NPs and each component of Fe, N, S, and C atoms over the entire sample were further supported by high-angle annular dark-field scanning transmission electron microscopy (HAADF-STEM) images and the corresponding energy-dispersive X-ray (EDX) elemental mapping analysis (Figure 1E). The atomic ratio of Fe and S was estimated to be 1:2.03 from EDX analysis, consistent with the stoichiometric pyrite FeS_2 (Figure 1F). To better confirm the formation of single-phase pyrite FeS_2 in FeS_2/NSC, ^{57}Fe Mössbauer spectroscopy was performed (Figure 2E) and showed the presence of only one paramagnetic doublet with chemical shift = 0.31 mm s^{-1} and quadrupole splitting = 0.62 mm s^{-1}, which is clear evidence for the formation of single-phase FeS_2 and consistent with FeS_2 with a pyrite structure.[17]

The surface elemental status of the FeS_2/NSC was further characterized by X-ray photoelectron spectroscopy (XPS). The $S 2p_{3/2}$ and $S 2p_{1/2}$ peaks (Figure 2C) observed at 162.7 and 163.8 eV, respectively, are consistent with the sulfur binding energy in bulk pyrite.[18] An intense peak at 164.9 eV corresponding to C—S—C bond was observed, indicating the successful incorporation of S atoms into the carbon framework.[19] Besides, two peaks around 168.8 eV assignable to the S—O oxidized species of sulfate were also detected, mainly owing to oxidation during storage.[10d] Note that no signals for elemental S at 164.0 ($2p_{3/2}$) and 165.2 eV ($2p_{1/2}$) were observed, demonstrating that the catalyst is free of elemental S impurities.[20] The Fe 2p spectrum (Figure 2D) shows a pair of spin-orbit split peaks at 707.4 ($2p_{3/2}$) and 720.1 eV ($2p_{1/2}$), respectively, which is consistent with the literature values for pyrite FeS_2.[21] Two less intensive shake-up peaks located at 711.6 and 725.6 eV were observed, assignable to the partial Fe^{3+}—S coordination bond and the surface oxidation states.[22] In addition, a signal at approximately 709.8 eV was also detected, which can be assigned

to Fe in Fe—N$_x$ configuration.[9a, 23] The high-resolution spectrum of C (Figure 2A) was fitted into five subpeaks, that is, C—C/C=C (284.7 eV), C—N (285.4 eV), C—S (286.6 eV), C—O (287.3 eV), and COOH (290.1),[24] verifying that the N and S atoms were incorporated into the porous carbon framework. Five types of N (Figure 2B), pyridinic N (398.5 eV, 15%), Fe—N$_x$ (399.6 eV, 16%),[25] pyrrolic N (400.9 eV, 37%), graphitic N (402.0 eV, 27%), and oxidized N (403.2 eV, 5%), could be distinguished from the N 1s spectrum. Notably, the appearance of the Fe—N$_x$ configuration in the sample from Fe 2p and N 1s XPS analysis implies the interaction of FeS_2 NPs with N atoms in the carbon framework.

N_2 adsorption/desorption measurements (Figure 2F) clearly demonstrate that FeS_2/NSC obtained with this preparation strategy possesses hierarchical micro-, meso-, and macropores, a high specific surface area (734.5 m^2 g^{-1}), and a large pore volume (0.408 cm^3 g^{-1}). Note that the hierarchical porous structure with a high specific surface area is expected to not only favor the reactant adsorption and rapid mass transfer but also provide good accessibility to the active sites, thereby boosting the catalytic performance.

Catalytic hydrogenation of nitroarenes

Catalytic hydrogenation of nitrobenzene (**1a**) was initially used as a model reaction to evaluate the catalytic activity of FeS_2/NSC. To pursue the reaction under milder, greener, and more sustainable conditions, the hydrogenation was first conducted at 120 °C under an H_2 pressure of 20 bar with water as solvent, and the results are shown in Table 1. To our delight, full conversion of **1a** to aniline (**2a**) was achieved within 5 h over

Table 1. Hydrogenation of nitrobenzene over FeS_2/NSC.[a]

Entry	Catalyst	T [°C]	P [bar]	Conv.[b] [%]	Sel.[b] [%]	TOF[c] [h^{-1}]
1	FeS_2/NSC	120	20	>99	100	4.4
2	FeS_2/NSC	100	20	53.6	100	2.3
3	FeS_2/NSC	80	20	35.2	100	1.5
4	FeS_2/NSC	120	10	84.9	100	3.7
5	FeS_2/SC	120	20	51.3	100	2.3
6	FeO$_x$/NC	120	20	37.5	100	1.7
7	CoS$_2$/NSC	120	20	84.9	100	3.7
8	NiS$_2$/NSC	120	20	41.4	100	1.8
9	Fe-phen/C-800	120	20	52.6	100	2.3
10	FeS_2	120	20	26.7	100	1.2
11	Fe$_2$O$_3$	120	20	17.5	100	0.77
12	Fe$_3$O$_4$	120	20	15.2	100	0.67
13	nano Fe powder	120	20	10.6	100	0.47
14[d]	–	120	20	3.7	100	0.16
15	NSC[e]	120	20	6	100	0.26

[a] Reaction conditions: nitrobenzene (0.5 mmol), catalyst (2.3 mol % Fe), H_2O (2 mL), H_2 (20 bar), 120 °C, 5 h. [b] Determined by GC with dodecane as an internal standard. [c] Turnover frequency (TOF) was calculated as moles of nitrobenzene converted divided by moles of metal per hour. [d] In the absence of any catalyst. [e] NSC represents N,S-codoped carbon with the same preparation procedure without addition of iron salt.
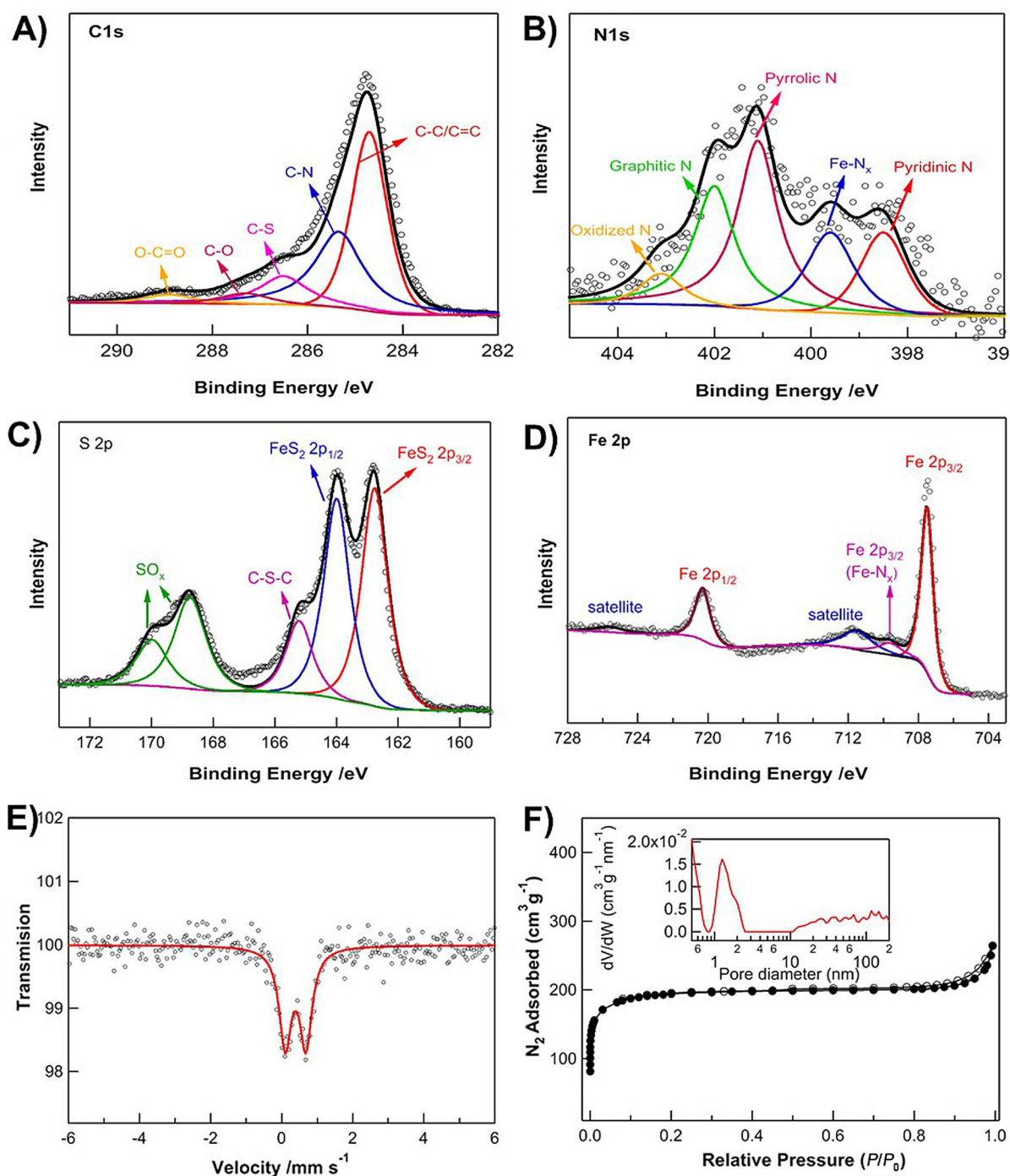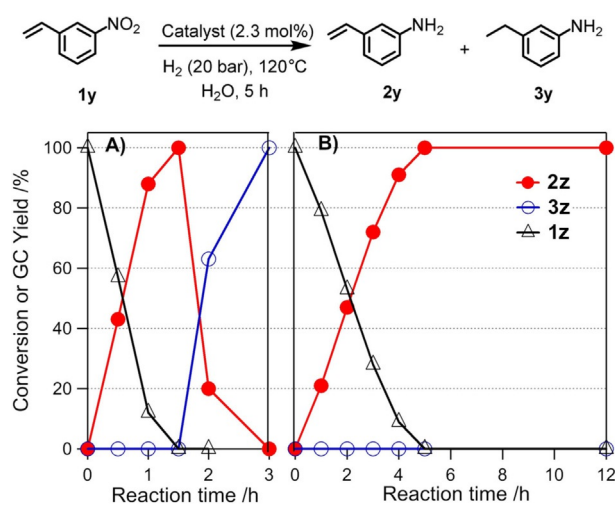
Figure 2. (A–D) XPS spectra of C 1s, N 1s, S 2p, and Fe 2p for FeS$_2$/NSC. (E) ^{57}Fe Mössbauer spectroscopy at 293 K and (F) N$_2$ adsorption isotherm of FeS$_2$/NSC.

FeS$_2$/NSC (entry 1). A decrease of reaction temperature or H$_2$ pressure resulted in significantly lower reaction efficiency (entries 2–4). With this impressive result in mind, a series of control experiments were subsequently performed. If NSC itself was used as the catalyst, only trace amounts of **2a** (6%) were observed (entry 14), demonstrating the almost inert nature of NSC for hydrogenation of nitrobenzene under the reaction conditions. Bulk FeS$_2$ as a catalyst delivered only 26.7% conversion of **1a** to **2a** under the same reaction conditions (entry 10). These two results indicate that the combination of

FeS$_2$ NPs and NSC is necessary to synergistically facilitate the reaction and achieve high reactivity. To prove this conclusion, FeS$_2$/SC without N-doping was prepared from commercially available activated carbon and employed as a catalyst for the model reaction. FeS$_2$/SC gave lower efficiency than FeS$_2$/NSC under otherwise identical conditions (entry 5), although its catalytic activity was still higher than that of bulk pyrite FeS$_2$ (entry 10). It should be noted that FeS$_2$/SC has a size of FeS$_2$ NPs similar to FeS$_2$/NSC, as shown in Figure S2 in the Supporting Information. In addition, a control test of the reaction in

the absence of catalyst under identical conditions only showed a negligible activity (entry 13), highlighting the critical role of FeS$_2$/NSC for the hydrogenation of nitroarenes. For comparison, other non-noble metal-based heterogeneous catalysts, Fe-phen/C-800,[8a] FeO$_x$/NC, CoS$_2$/NSC, and NiS$_2$/NSC (entries 6–9), were also employed as catalysts for the reaction, and none of them surpassed the reaction efficiency of FeS$_2$/NSC. Particularly, Fe-phen/C-800 and FeO$_x$/NC, which consist of Fe$_2$O$_3$ NPs as major phases, showed rather lower catalytic activity than FeS$_2$/NSC under the present conditions (entry 9). Taking into account these results, we can come to a conclusion that the large specific surface area, high pore volume, and N,S codoping of the carbon framework substantially contribute to the enhanced catalytic performance.

After identifying the optimized reaction conditions, we further applied FeS$_2$/NSC for hydrogenation of the most demanding 4-iodonitrobenzene (**1 x**) and 3-nitrostyrene (**1 z**) among a variety of functionalized nitroarenes, owing to their considerably inclination towards C=C bond reduction and dehalogenation. To our delight, FeS$_2$/NSC not only showed high activity for both reactants but more importantly a selectivity greater than 99 % at full conversion towards their respective desired productes, 4-iodoaniline (**2 x**) and 3-aminostyrene (**2 z**), without observation of any reduction of C=C bond or dehalogenation even at prolonged reaction times (Figure 3). These results are significantly different from those exhibited by platinum-group catalysts, for which low chemoselectivity to the desired amines was usually achieved after full conversion of **1 x** and **1 z**. For example, the commercially available Pd/C gave the complete over-reduction product 3-ethylaniline (**3 z**) after full conversion at slightly prolonged times, although it exhibited rather higher reaction efficiency (Figure 3 A). Notably, in the case of hydrogenation of **1 z**, 96 % isolated yield with a turnover frequency (TOF) as high as 8.4 h^{-1} was achieved, which is 42 and 120 times higher than those catalyzed by bulk pyrite FeS$_2$ reported by Schaak and co-workers and Keil and co-workers (Table S3 in the Supporting Information),[11] respectively. To the

best of our knowledge, this is the highest value among many state-of-the-art nonprecious metal-based heterogeneous catalysts (Table S3 in the Supporting Information). More importantly, the reaction conditions (20 bar H$_2$, 120 °C, 5 h, water as solvent) in this case are comparatively much milder and greener than those previous reports, making the process more operationally practical and cost-effective.

Subsequently, we further explored the generality of FeS$_2$/NSC for other functionalized nitroarenes. Overall, FeS$_2$/NSC showed outstanding tolerance towards a broad spectrum of substituted nitroarenes, as demonstrated in Table 2. Various functional groups are compatible with the present reaction conditions, especially for those bearing aldehyde (**1 s**), ketone (**1 u**), ester (**1 v**), amide (**1 t**), nitrile (**1 w**), and halide (e.g., **1 g**–**j**, **1 x**) groups. In all cases listed in Table 2, high activity with exclusive selectivity to the corresponding anilines was observed without detection of the reduction of these reducible groups

Figure 3. Comparison of 3-nitrostyrene hydrogenation over (A) commercial Pd/C and (B) FeS$_2$/NSC.

Table 2. Substrate scope.[a]

2a (99%), 2b (99%), 2c (98%), 2d (99%), 2e (98%)
2f (99%), 2g (99%), 2h (94%), 2i (98%), 2j (99%)
2k (99%), 2l (99%), 2m (98%), 2n (93%), 2o (96%)
2p (96%), 2q (93%), 2r (97%)
2s (96%), 2t (98%), 2u (97%)
2v (98%), 2w (99%), 2x (98%)
2y (98%), 2z (96%), 2ab (96%)
2ac (91%), 2ad (84%), 2ae (83%)

[a] Reaction conditions: nitroarene (0.5 mmol), FeS$_2$/NSC (2.3 mol % Fe), H$_2$O (2 mL), H$_2$ (20 bar), 120 °C, 5 h. Isolated yields.

or dehalogenation. Furthermore, this protocol is also applicable for heteroatom-containing nitro compounds, such as 3-nitropyridine (**1q**) and 5-nitroquinoline (**1r**), affording their respective anilines in high yields. In addition, marketed nitro-substituted drugs, for example, Nimodipine (**1ac**), Nilutamide (**1ad**), and Niclosamide (**1ae**), were hydrogenated to their corresponding amines in high isolated yields with excellent selectivity.

Durability and recyclability of a catalyst are important features for the advancement of sustainable practical processes. Upon completion of the hydrogenation of 3-nitrostyrene, FeS_2/NSC was recollected by centrifugation, washed, and dried for reuse in subsequent cycles. As shown in Figure S3 in the Supporting Information, FeS_2/NSC was highly stable and could be conveniently recycled up to eight times to chemoselectively produce 3-aminostyrene without any loss of selectivity, although the activity decreased slightly. No significant difference was observed for FeS_2/NSC before and after the reaction by Raman and elemental analysis, clearly indicating its strong stability (Figure S4 and Table S4 in the Supporting Information).

Mechanism of catalysis by FeS_2/NSC

To unveil the underlying factors that provide the excellent activity and superior selectivity in the hydrogenation of nitroarenes, some control experiments were performed. First, we performed the hydrogenation of styrene over FeS_2/NSC under the optimized conditions. As shown in Scheme 2, the catalysts FeS_2/NSC, FeO_x/NC, and FeS_2/SC all showed negligible activity with almost complete recovery of styrene. However, high activity was achieved for the hydrogenation of nitrobenzene as shown in Table 1. Furthermore, if a mixture (1:1) of styrene and nitrobenzene was subjected to the optimized conditions, only aniline was observed in quantitative yield whereas the C=C bond in styrene remained untouched. These results clearly demonstrate that FeS_2/NSC was intrinsically active for the hydrogenation of the nitro group, most likely owing to the preferential adsorption of the nitro group over the olefinic group. Second, we performed attenuated total reflection (ATR-)IR spectroscopy to study the adsorption behavior of FeS_2/NSC for both nitro and olefinic groups (Figure 4). Two clear peaks at approximately 1346 and 1524 cm^{-1} were present after adsorp-
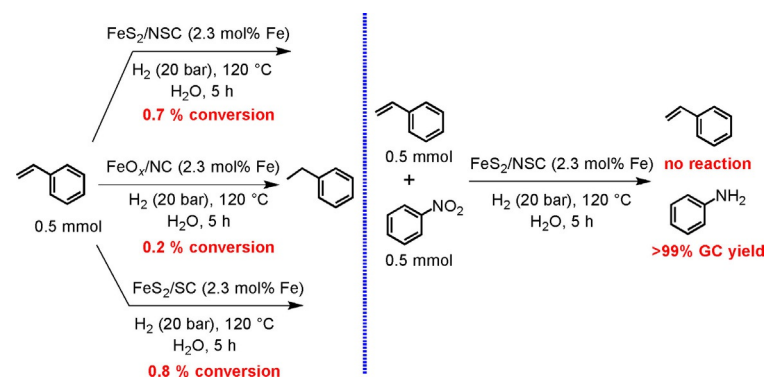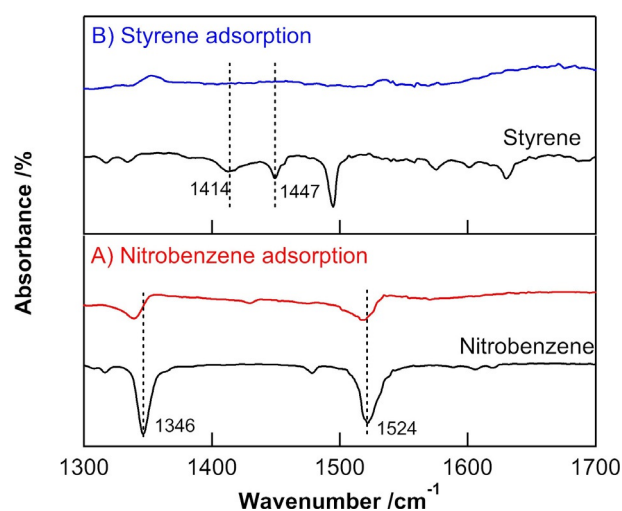
Figure 4. ATR-IR spectra for (A) nitrobenzene and (B) styrene adsorption behavior over FeS_2/NSC.

tion of nitrobenzene on FeS_2/NSC, which can be assigned to the asymmetrical stretch of the NO_2 group.[8a,b] In contrast, no characteristic peaks assignable to the C=C group were observed after adsorption of styrene on FeS_2/NSC. These IR results demonstrate that FeS_2/NSC preferentially adsorbs the nitro group rather than the olefinic group, which is line with the results of the hydrogenation of nitrobenzene and styrene under the same reaction conditions. It has been well documented that heteroatoms (e.g., N, S, or P) doped on carbon could effectively tune electron redistribution at the interface of heteroatom-doped carbon and metal immobilized or encapsulated on carbon, and in turn could enrich the positive charges on the side of metal through the Mott–Schottky effect.[26] As a consequence, the large electronegative N and S atoms co-incorporated in the carbon make the single-phase FeS_2 nanoparticles more positively charged, which is more favorable for the adsorption of the nitro group owing to its strong electron-withdrawing nature. In addition, H_2 temperature-programmed reduction (TPR) experiments for FeS_2/NSC suggested that FeS_2 NPs have a relatively strong interaction with N,S-codoped carbon (Figure 5), which was also evidenced by the observation of Fe-N$_x$ configuration in Fe 2p and N 1s XP spectra.

To obtain deeper insight into the unique catalytic behavior of FeS_2/NSC, periodic DFT calculations were performed. The pyrite FeS_2 (200) facet and the positively charged FeS_2 (200) facet were adopted as models for representing FeS_2 and FeS_2/NSC. It is well known that the activation of molecular H_2 and adsorption modes of 3-nitrostyrene or other functionalized nitroarenes on the catalysts have profound influence on the activity and selectivity for hydrogenation of nitroarenes. As shown in Figure 3, the product distribution of the hydrogenation of 3-nitrostyrene as a function of reaction times revealed that the reaction proceeds in a direct way without detection of any intermediate. As such, we first calculated the dissociation energy for molecular hydrogen on both bulk
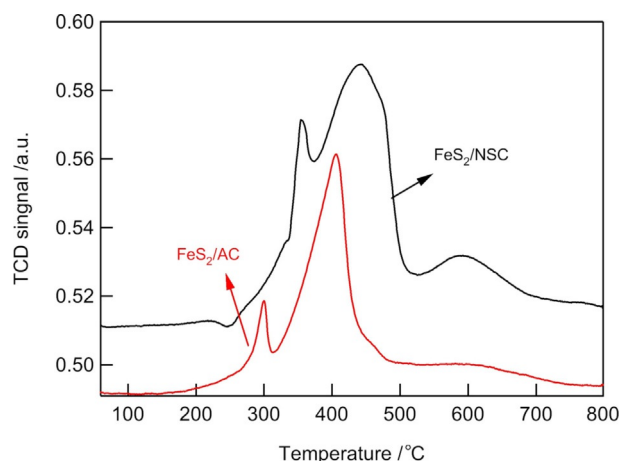

Scheme 2. Comparison of selected supported iron catalysts for the hydrogenation of styrene.

Figure 5. H$_2$-TPR profile for FeS$_2$/SC and FeS$_2$/NSC.

FeS$_2$ (200) and positively charged FeS$_2$ (200). In this case, only a slight difference (≈ 0.02 eV) between two models with a dissociation energy of 0.30 and 0.28 eV, respectively, was observed (Figure S5 in the Supporting Information). This observation indicated that the formation of a single-phase pyrite FeS$_2$ NPs on N,S-codoped carbon did not have a great effect on the activation of H$_2$ on the surface of catalyst. Thus, the contribution from H$_2$ activation for the highly boosted reaction efficiency could be ruled out. Subsequently, DFT calculations for the adsorption energy of 3-nitrostyrene on both models were performed to study the interaction between nitro or olefinic groups and the catalysts. As shown in Figure 6, -0.33 and -0.50 eV adsorption energies were observed for adsorption through the C=C and NO$_2$ groups with FeS$_2$ (200), respectively, strongly suggesting a more preferential adsorption through the nitro group. This phenomenon was further reinforced for the adsorption on positively charged FeS$_2$ (200). In this case, the calculated adsorption energy of -1.09 eV for the adsorp-
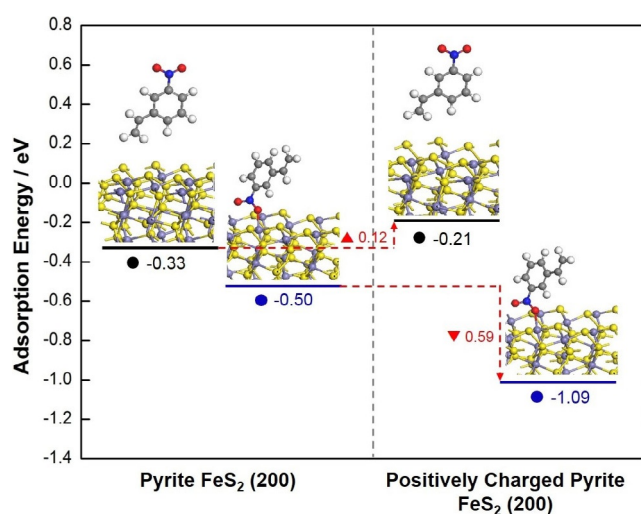
tion through the nitro group was obtained, which is two times higher than that on the FeS$_2$ (200) surface. In contrast, a much lower adsorption energy of -0.21 eV for the adsorption through the C=C group was obtained, indicating a less stable adsorption on the surface. Consequently, DFT calculations clearly disclosed that the positively charged FeS$_2$ NPs greatly enhance adsorption of the nitro group. This is also in good agreement with the results of ATR-IR spectroscopy and the hydrogenation reactions. Taking into account computational and control experiment results together, the unique features of preferential adsorption of the nitro group together with the large specific surface area, hierarchical pores, high pore volume, and strong metal–support interaction shown by FeS$_2$/NSC account for the enhanced activity and exclusive selectivity in the hydrogenation of functionalized nitroarenes.

Conclusions

Single-phase pyrite FeS$_2$ nanoparticles supported on N,S-codoped hierarchical porous carbon (FeS$_2$/NSC) were fabricated in a straightforward and cost-effective process. FeS$_2$ nanoparticles with uniform size were homogeneously dispersed on N,S-codoped porous carbon derived from biomass with high specific surface area, hierarchical pores, and large pore volume. The resultant FeS$_2$/NSC exhibited outstanding catalytic activity and exclusive selectivity for catalytic hydrogenation of various functionalized nitroarenes with a broad spectrum of functional groups. Significantly, a remarkable enhancement in catalytic activity was achieved compared with the bulk FeS$_2$ or other non-noble metal-based catalysts under milder reaction conditions in water. DFT calculations disclosed that FeS$_2$/NSC has a preferential adsorption of the nitro group, which accounts for the highly boosted activity and superior selectivity. In addition, the FeS$_2$/NSC demonstrated a high stability and could be recycled up to 8 times without an appreciable loss in catalytic performance. This work represents an important advance for boosting the catalytic performance by combination of a non-noble metal with heteroatom-doped porous carbon materials.

Acknowledgements

Conflict of interest

The authors declare no conflict of interest.

Keywords: chemoselectivity · functionalized nitroarenes · hydrogenation · N,S-codoped porous carbon · pyrite FeS$_2$

Figure 6. Adsorption energy of 3-nitrostyrene on pyrite FeS$_2$ (200) and positively charged FeS$_2$ (200) surface. Color index: Fe=gray; S=yellow; C=dark gray; N=blue; O=red; H=white.

[1] a) N. Ono, *The Nitro Group in Organic Synthesis* (Ed.: H. Feuer), Wiley-VCH, Weinheim, **2001**; b) H. U. Balser, U. Siegrist, H. Steiner, *Aromatic Nitro Compounds, in Fine Chemicals Through Heterogeneous Catalysis* (Eds.: R. A. Sheldon, H. van Bekkum), Wiley-VCH, Weinheim, **2001**; c) R. S. Downing, P. J. Kunkeler, H. Bekkum, *Catal. Today* **1997**, *37*, 121.

[2] D. Formenti, F. Ferretti, F. K. Scharnagl, M. Beller, *Chem. Rev.* **2019**, *119*, 2611.

[3] A. Corma, P. Serna, *Science* **2006**, *313*, 332.

[4] a) H.-S. Wei, X.-Y. Liu, A.-Q. Wang, L. Zhang, B.-T. Qiao, X.-F. Huang, S. Miao, J.-Y. Liu, T. Zhang, *Nat. Commun.* **2014**, *5*, 5634; b) J. Gu, Z.-Y. Zhang, P. Hu, L.-P. Ding, N.-H. Xue, L.-M. Peng, X.-F. Guo, M. Lin, W.-P. Ding, *ACS Catal.* **2015**, *5*, 6893; c) H. Wei, Y. Ren, A. Wang, X. Liu, X. Liu, L. Zhang, S. Miao, L. Li, J. Liu, J. Wang, G. Wang, D. Su, T. Zhang, *Chem. Sci.* **2017**, *8*, 5126.

[5] a) Y. Chen, C. Wang, H. Liu, J. Qiu, X.-H. Bao, *Chem. Commun.* **2005**, 5298; b) K. Shimizu, Y. Miyamoto, A. Satsuma, *J. Catal.* **2010**, *270*, 86; c) T. Mitsudome, Y. Mikami, M. Matoba, T. Mzugaki, K. Jitukawa, K. Kaneda, *Angew. Chem. Int. Ed.* **2012**, *51*, 136; *Angew. Chem.* **2012**, *124*, 140.

[6] a) S. Zhang, C.-R. Chang, Z.-Q. Huang, J. Li, Z. Wu, Y. Ma, Z. Zhang, Y. Wang, Y. Qu, *J. Am. Chem. Soc.* **2016**, *138*, 2629; b) J. Zhang, L. Wang, Y. Shao, Y. Wang, B. C. Gates, F.-S. Xiao, *Angew. Chem. Int. Ed.* **2017**, *56*, 9747; *Angew. Chem.* **2017**, *129*, 9879; c) M. Guo, H. Li, Y.-Q. Ren, X. M. Ren, Q.-H. Yang, C. Li, *ACS Catal.* **2018**, *8*, 6476; d) C. Wang, L. Wang, J. Zhang, H. Wang, J. P. Lewis, F.-S. Xiao, *J. Am. Chem. Soc.* **2016**, *138*, 7880.

[7] I. Nakamula, Y. Yamanoi, T. Imaoka, K. Yamamoto, H. Nishihara, *Angew. Chem. Int. Ed.* **2011**, *50*, 5830; *Angew. Chem.* **2011**, *123*, 5952.

[8] a) A. Corma, P. Concepción, P. Serna, *Angew. Chem. Int. Ed.* **2007**, *46*, 7266; *Angew. Chem.* **2007**, *119*, 7404; b) M. Boronat, P. Concepción, S. González, F. Illas, P. Serna, *J. Am. Chem. Soc.* **2007**, *129*, 16230; c) Y. Tan, X.-Y. Liu, L. Zhang, A. Wang, L. Li, X. Pan, S. Miao, M. Haruta, H. Wei, H. Wang, F. Wang, X. Wang, T. Zhang, *Angew. Chem. Int. Ed.* **2017**, *56*, 2709; *Angew. Chem.* **2017**, *129*, 2753; d) L. Wang, E.-J. Guan, J. Zhang, J.-H. Yang, Y.-H. Zhu, Y. Han, M. Yang, C. Cen, G. Fu, B. C. Gates, F.-S. Xiao, *Nat. Commun.* **2018**, *9*, 1362.

[9] a) R. V. Jagadeesh, A.-E. Surkus, H. Junge, M.-M. Pohl, J. Radnik, J. Rabeah, H.-M. Huan, V. Schünemann, A. Brückner, M. Beller, *Science* **2013**, *342*, 1073; b) R. V. Jagadeesh, T. Stemmler, A.-E. Surkus, H. Junge, K. Junge, M. Beller, *Nat. Protoc.* **2015**, *10*, 548; c) F. A. Westerhaus, R. V. Jagadeesh, G. Wienhöfer, M.-M. Pohl, J. Radnik, A.-E. Surkus, J. Rabeah, K. Junge, H. Junge, M. Nielsen, M. Beller, *Nat. Chem.* **2013**, *5*, 537.

[10] a) C. Wadia, A. Paul Alivisatos, D. M. Kammen, *Enivron. Sci. Technol.* **2009**, *43*, 2072; b) M. Cabán-Acevedo, D. Liang, K.-S. Chew, J. P. De-Grave, N. S. Kaiser, S. Jing, *ACS Nano* **2013**, *7*, 1731; c) D.-Y. Wang, M. Gong, H.-L. Chou, C.-J. Pan, H.-A. Chen, Y.-P. Wu, M.-C. Lin, M.-Y. Guan, J. Yang, C.-W. Chen, Y.-L. Wang, B.-J. Hwang, C.-C. Chen, H.-J. Dai, *J. Am. Chem. Soc.* **2015**, *137*, 1587; d) Z. Guo, X.-W. Wang, *Angew. Chem. Int. Ed.* **2018**, *57*, 5898; *Angew. Chem.* **2018**, *130*, 6000; e) M. Lashgari, P. Zei-nalkhani, *Nano Energy* **2018**, *48*, 361; f) Y.-C. Wang, D.-Y. Wang, Y.-T. Jiang, H.-A. Chen, C.-C. Chen, K.-C. Ho, H.-L. Chou, C.-W. Chen, *Angew. Chem. Int. Ed.* **2013**, *52*, 6694; *Angew. Chem.* **2013**, *125*, 6826; g) N. Voronina, H. Yashiro, S.-T. Myung, *J. Mater. Chem. A* **2018**, *6*, 17111; h) Z.-Q. Sun, H.-M. Lin, F. Zhang, X. Yang, H. Jiang, Q. Wang, F.-Y. Qu, *J. Mater. Chem. A* **2018**, *6*, 14956; i) Y.-X. Li, J. Yin, L. An, M. Lu, K. Sun, Y.-Q. Zhao, D.-Q. Gao, F.-Y. Cheng, P.-X. Xi, *Small* **2018**, *14*, 1801070; j) R.-W. Wang, M. Yan, H.-D. Li, L. Zhang, B.-Q. Peng, J.-Z. Sun, D. Liu, S.-Q. Liu, *Adv. Mater.* **2018**, *30*, 1800618; k) A. Douglas, R. Carter, L. Oakes, K. Share, A. P. Cohn, C. L. Pint, *ACS Nano* **2015**, *9*, 11156; l) S. Shukla, J. W. Ager, Q. Xiong, T. Sritharan, *Energy Technol.* **2018**, *6*, 8.

[11] a) J. R. Morse, J. F. Callejas, A. J. Darling, R. E. Schaak, *Chem. Commun.* **2017**, *53*, 4807; b) B. Ma, X.-L. Tong, C.-X. Guo, X.-N. Guo, X.-Y. Guo, F. J. Keil, *RSC Adv.* **2016**, *6*, 55220.

[12] a) Z.-Z. Wei, S.-J. Mao, F.-F. Sun, J. Wang, B.-B. Mei, Y.-Q. Chen, H.-R. Li, Y. Wang, *Green Chem.* **2018**, *20*, 671; b) Y.-D. Shao, Z. Guo, H. Li, Y.-T. Su, X.-W. Wang, *Angew. Chem. Int. Ed.* **2017**, *56*, 3226; *Angew. Chem.* **2017**, *129*, 3274.

[13] C. Wadia, Y. Wu, S. Gul, S. K. Volkman, J. Guo, A. Paul Alivisatos, *Chem. Mater.* **2009**, *21*, 2568.

[14] a) T. Song, P. Ren, Y.-N. Duan, Z.-Z. Wang, X.-F. Chen, Y. Yang, *Green Chem.* **2018**, *20*, 4629; b) Y.-N. Duan, T. Song, X.-S. Dong, Y. Yang, *Green Chem.* **2018**, *20*, 2821; c) X.-S. Dong, Z.-Z. Wang, Y.-N. Duan, Y. Yang, *Chem. Commun.* **2018**, *54*, 8913; d) T. Song, Z.-M. Ma, Y. Yang, *Chem-CatChem* **2019**, *11*, 1313; e) B. Sahoo, C. Kreyenschulte, G. Agostini, H. Lund, S. Bachmann, M. Scalone, K. Junge, M. Beller, *Chem. Sci.* **2018**, *9*, 8134; f) W. Liu, L. Zhang, W. Yan, X. Liu, X. Yang, S. Miao, W. Wang, A. Wang, T. Zhang, *Chem. Sci.* **2016**, *7*, 5758; g) P. Zhou, Z. Zhang, *ChemSusChem* **2017**, *10*, 1892; h) R. V. Jagadeesh, K. Murugesan, A. S. Alsham-mari, H. Neumann, M.-M. Pohl, J. Radnik, M. Beller, *Science* **2017**, *358*, 326; i) Z. Z. Wei, J. Wang, S. J. Mao, D. F. Su, H. Y. Jin, Y. H. Wang, F. Xu, H. R. Li, Y. Wang, *ACS Catal.* **2015**, *5*, 4783; j) K. Shen, L. Chen, J. L. Long, W. Zhong, Y. W. Li, *ACS Catal.* **2015**, *5*, 5264; k) H. T. Schwob, R. Kempe, *Angew. Chem. Int. Ed.* **2016**, *55*, 15175; *Angew. Chem.* **2016**, *128*, 15400; l) X. Ma, Y. X. Zhou, H. Liu, Y. Li, H.-L. Jiang, *Chem. Commun.* **2016**, *52*, 7719; m) G. Hahn, P. Kunnas, N. de Jonge, R. Kempe, *Nat. Catal.* **2019**, *2*, 71–77; n) F. Yang, M. Wang, W. Liu, B. Yang, Y. Wang, J. Luo, Y. Tang, L. Hou, Y. Li, Z. Li, B. Zhang, W. Yang, Y. Li, *Green Chem.* **2019**, *21*, 704.

[15] D. Mhamane, W. Ramadan, M. Fawzy, A. Rana, M. Dubey, C. Rode, B. Lefez, B. Hannoyerd, S. Ogale, *Green Chem.* **2011**, *13*, 1990.

[16] M. Cabán-Acevedo, M. S. Faber, Y.-Z. Tan, R. J. Hamers, S. Jin, *Nano Lett.* **2012**, *12*, 1977.

[17] a) P. P. Chin, J. Ding, J. B. Yi, B. H. Liu, *J. Alloys Compd.* **2005**, *390*, 255; b) J. P. Eymery, *Eur. Phys. J. Appl. Phys.* **1999**, *5*, 115.

[18] L. Xu, Y. Hu, H. Zhang, H. Jiang, C. Li, *ACS Sustainable Chem. Eng.* **2016**, *4*, 4251.

[19] J. Liang, Y. Jiao, M. Jaroniec, S.-Z. Qiao, *Angew. Chem. Int. Ed.* **2012**, *51*, 11496; *Angew. Chem.* **2012**, *124*, 11664.

[20] J. F. Moulder, W. K. Stickle, P. E. Sobol, K. D. Bomben, *Handbook of X-ray Photoelectron Spectroscopy*, Perkin-Elmer Corp., Physical Electronics Inc., Eden Prairie, Minnesota, **1995**.

[21] W. Chen, S. Qi, L. Guan, C. Liu, S. Cui, C. Shen, *J. Mater. Chem. A* **2017**, *5*, 5332.

[22] Y. Xin, Z. Li, W. Wu, B. Fu, Z. Zhang, *ACS Sustainable Chem. Eng.* **2016**, *4*, 6659.

[23] R.-G. Cao, R. Thapa, H.-J. Kim, X.-D. Xu, M. G. Kim, Q. Li, N. Park, M.-L. Liu, J. Cho, *Nat. Commun.* **2013**, *4*, 2076.

[24] H. Tao, C. Yan, A. W. Robertson, Y. Gao, J. Ding, Y. Zhang, T. Ma, Z. Sun, *Chem. Commun.* **2017**, *53*, 873–876.

[25] W.-J. Jiang, L. Gu, L. Li, Y. Zhang, X. Zhang, L.-J. Zhang, J.-Q. Wang, J.-S. Hu, Z. Wei, L.-J. Wan, *J. Am. Chem. Soc.* **2016**, *138*, 3570.

[26] X. H. Li, M. Antonietti, *Chem. Soc. Rev.* **2013**, *42*, 6593.